Uluslararası İleri Doğa Bilimleri ve Mühendislik Araştırmaları Dergisi
Sayı 9, S. 147-157, 8, 2025

Araştırma Makalesi

IJANSER
https://as-proceeding.com/index.php/ijanser
ISSN:2980-0811

International Journal of Advanced Natural Sciences and Engineering Researches
Volume 9, pp. 147-157, 8, 2025

Research Article

Aerodynamic Performance Analysis of a Main Propeller with Jointed Tip-Mounted Blades Using Extended Blade Element Momentum Theory

Osman ACAR*

[1]*Department of Mechanical Engineering, Faculty of Technology, Selcuk University, Turkiye*

*(osmanacar@selcuk.edu.tr) *Email of the corresponding author*

(Received: 09 August 2025, Accepted: 16 August 2025)

(6th International Conference on Engineering, Natural and Social Sciences ICENSOS 2025, August 10-11, 2025)

ATIF/REFERENCE: Acar, O. (2025). Aerodynamic Performance Analysis of a Main Propeller with Jointed Tip-Mounted Blades Using Extended Blade Element Momentum Theory, *International Journal of Advanced Natural Sciences and Engineering Researches*, 9(8), 147-157.

Abstract – This study presents a comprehensive computational framework for evaluating the aerodynamic performance of a primary propeller system integrated with tip-mounted secondary propellers, aimed at mission adaptability without decreasing propulsion efficiency. The analytical model is grounded in the Blade Element Momentum (BEM) method, augmented with Prandtl's tip-loss correction to accurately capture finite blade effects, and employs an iterative inflow solution scheme to ensure convergence of induced velocity predictions. The formulation resolves aerodynamic forces at a fine spanwise resolution, enabling detailed insight into the distribution of lift, drag, and local angles of attack along both the main and secondary propeller blades. A distinctive feature of the configuration is the mechanical joint of the secondary propellers to the primary blade rotation, resulting in each tip-mounted rotor experiencing a complex effective freestream velocity composed of the aircraft's translational speed and the tangential velocity at the primary blade tips. The MATLAB-based implementation of the model provides thrust, torque, and propulsive efficiency curves, as well as high-fidelity aerodynamic load maps for both the main and secondary blades. Three-dimensional visualizations are generated to illustrate the spatial loading patterns and aerodynamic interactions across the operational envelope. Results for a representative baseline geometry demonstrate the influence of tip-mounted propellers on total thrust augmentation, torque demand, and efficiency trends. The proposed methodology offers a rapid and reliable tool for preliminary design optimization of unconventional multi-propeller architectures, significantly reducing the reliance on computationally intensive CFD simulations while maintaining a high degree of predictive accuracy.

Keywords –Blade Element Momentum, Tip-Mounted Propellers, Prandtl Tip Loss, Propeller Aerodynamics, MATLAB Simulation.

I. INTRODUCTION

The pursuit of mission adaptability without decreasing propulsive efficiency in rotary-wing and propeller-driven systems has led to innovative blade tip designs that aim to recover energy from the high tangential velocity region near the blade tips. Traditional propeller designs suffer from tip vortex formation and associated induced drag, which can reduce overall aerodynamic efficiency [1], [2]. In

recent years, unconventional tip devices such as winglets, swept tips, and multi-jointed tip blades have been proposed to mitigate these losses and potentially extract additional useful thrust [3–5].

Among these approaches, the concept of tip-mounted propellers, small auxiliary propellers integrated at the tips of the main rotor or propeller blades, has gained attention for its ability to utilize the high rotational speed at the tip radius. This configuration has the potential to generate additional thrust without requiring a proportional increase in shaft power input, thereby improving the power-to-thrust ratio [6]. However, the aerodynamic interactions between the main and tip-mounted propellers can be complex, as the tip propeller operates in a highly non-uniform inflow field with significant tangential velocity components [7], [8].

Previous experimental and computational studies have investigated propeller performance enhancement through various tip modifications. For example, blade tip winglets have been shown to reduce induced losses by redirecting the tip vortex [9], while actively powered tip devices have demonstrated thrust augmentation at certain operating conditions [10]. However, most of these studies either considered stationary or mechanically geared tip propellers, or relied on simplified inflow assumptions that do not fully capture the relative velocity environment of a free-rotating jointed tip propeller [11], [12].

The present study addresses this gap by applying an extended Blade Element Momentum (BEM) theory to a main propeller with jointed tip-mounted blades, in which the tip blades are hinged at the end of the main blades and rotate freely in response to the aerodynamic loads and the effective inflow velocity. The analysis focuses on deriving the effective freestream velocity for the tip-mounted propellers as the vector sum of the main blade tangential speed and the aircraft forward velocity, providing a more realistic representation of the aerodynamic environment [13].

A MATLAB-based computational model was developed to evaluate the thrust, power, and propulsive efficiency of both the main and tip-mounted propellers over a wide range of forward speeds. The model incorporates performance coefficient data for the propeller sections and resolves the interactions between the main and tip-mounted components. The study aims to:

Quantify the net thrust and efficiency changes due to the addition of jointed tip-mounted blades.

Identify the operating conditions under which tip-mounted blades produce positive, neutral, or negative thrust.

Provide guidance for design optimization, including potential benefits of variable pitch or adaptive control.

This paper is structured as follows: Section 2 describes the methodology and the extended BEM formulation, including the derivation of the effective tip propeller inflow velocity. Section 3 presents the results of the MATLAB simulations, including the complete performance summary table and graphical performance curves. Section 4 discusses the aerodynamic implications of the results and proposes design improvements. Finally, Section 5 summarizes the main conclusions and suggests directions for future work.

II. MATERIALS AND METHOD

The aerodynamic analysis was conducted using an extended Blade Element Momentum (BEM) theory to account for the coupled performance of the main propeller and the jointed tip-mounted propeller. The BEM framework was chosen for its balance between computational efficiency and the ability to capture key aerodynamic phenomena [14], [15].

The model treats the main and tip-mounted propellers as separate rotor systems, each subdivided into radial elements. For each element, the local inflow velocity, angle of attack, and resulting aerodynamic forces are computed, then integrated over the span to obtain total thrust and torque. The tip-mounted propeller analysis incorporates the tangential velocity from the main propeller tip as a component of its effective freestream velocity.

A. Blade Element Momentum Theory for Main Propeller

Level-2 and level-3 headings can be used to detail main headings. The main propeller is divided into N annular blade elements of width d_r, each at radius r from the rotation axis. For each element, the relative velocity is given by:

$$V_{rel,main}(r) = \sqrt{(V_\infty(1-a))^2 + (\Omega r(1+a'))^2}$$

where:

a = axial induction factor

a' = tangential induction factor

The elemental thrust and torque are then computed as:

$$dT_{main} = \frac{1}{2}\rho {V_{rel,main}}^2 c(r) C_L(r) cos\phi dr$$

$$dQ_{main} = \frac{1}{2}\rho {V_{rel,main}}^2 c(r) C_D(r) r dr$$

where:

- $c(r)$= chord length at radius r
- $C_L(r),\ C_D(r)$= local lift and drag coefficients
- ϕ = inflow angle

4. **Elemental thrust and torque:**

$$dT = dL\cos\phi - dD\sin\phi$$

$$dQ = (dL\sin\phi + dD\cos\phi)r$$

These are summed across all elements and blades to yield total thrust and torque.

2.2 Prandtl Tip Loss Correction

To account for finite blade effects:

$$F = \frac{2}{\pi}\cos^{-1}\left[\exp\left(\frac{-B}{2}\frac{R-r}{r\sin\phi}\right)\right]$$

This correction is applied iteratively in the inflow solution to improve accuracy near the tip.

The total thrust and power are obtained by integrating over the radius:

$$T_{main} = B\int_{r_{hub}}^{R_{main}} dT_{main}$$

$$P_{main} = 2\pi\Omega\int_{r_{hub}}^{R_{main}} dQ_{main}$$

where B is the number of main propeller blades.

B. Effective Freestream Velocity for Tip-Mounted Propeller

The jointed tip-mounted propeller experiences a combined inflow consisting of the axial freestream velocity V_∞ and the tangential velocity from the main propeller tip ΩR_{main}. Assuming the tip-mounted propeller axis is oriented perpendicular to the main propeller blade, the effective freestream velocity is:

$$V_{eff,tip} = \sqrt{V_\infty^2 + (\Omega R_{main})^2}$$

This formulation assumes no mechanical gearing; the tip-mounted blade rotation results purely from aerodynamic loading in the high-speed tip flow. The relative velocity at each tip propeller element is then:

$$V_{rel,tip}(r_t) = \sqrt{(V_{eff,tip}(1-a_t))^2 + (\Omega_t r_t(1+a'_t))^2}$$

where r_t is the radial coordinate along the tip-mounted blade, Ω_t is the angular velocity of the tip propeller, and a_t, a'_t are its axial and tangential induction factors.

C. Aerodynamic Force and Power Calculation for Tip Propeller

Using the same BEM element formulation, the elemental thrust and torque for the tip-mounted propeller are:

$$dT_{tip} = \frac{1}{2}\rho {V_{rel,tip}}^2 c_t(r_t) C_{L,t}(r_t) cos\phi dr$$

$$dQ_{tip} = \frac{1}{2}\rho {V_{rel,tip}}^2 c_t(r_t) C_{D,t}(r_t) r_t dr_t$$

The integrated quantities yield total thrust and power:

$$T_{tip} = B_t \int_{r_{hub,t}}^{R_{tip}} dT_{tip}$$

$$P_{tip} = 2\pi\Omega_t \int_{r_{hub,t}}^{R_{tip}} dQ_{tip}$$

where B_t is the number of tip propeller blades.

D. Efficiency Metrics

The propulsive efficiencies are computed as:

$$\eta_{main} \frac{T_{main} V_\infty}{P_{main}}$$

$$\eta_{tip} \frac{T_{tip} V_\infty}{P_{tip}}$$

$$\eta_{total} \frac{(T_{main} + T_{tip}) V_\infty}{P_{main} + P_{tip}}$$

Negative thrust values correspond to the tip-mounted propeller acting as a drag device rather than a thrust generator. The computational model was implemented in MATLAB, allowing parametric sweeps over the forward speed V_∞. At each speed, the program calculated thrust, torque, and efficiency for both the main and tip propellers using pre-defined aerodynamic coefficients. The model output included numerical performance table (31 data points), plots of thrust vs. forward speed, power vs. forward speed, and efficiency vs. forward speed, separate contributions of main and tip propellers for comparison. A schematic illustrating the geometry of the main blade with its jointed tip-mounted propeller is shown in Fig. 1. This diagram defines all relevant parameters, including R_{main}, R_{tip}, and velocity components used in the derivations.

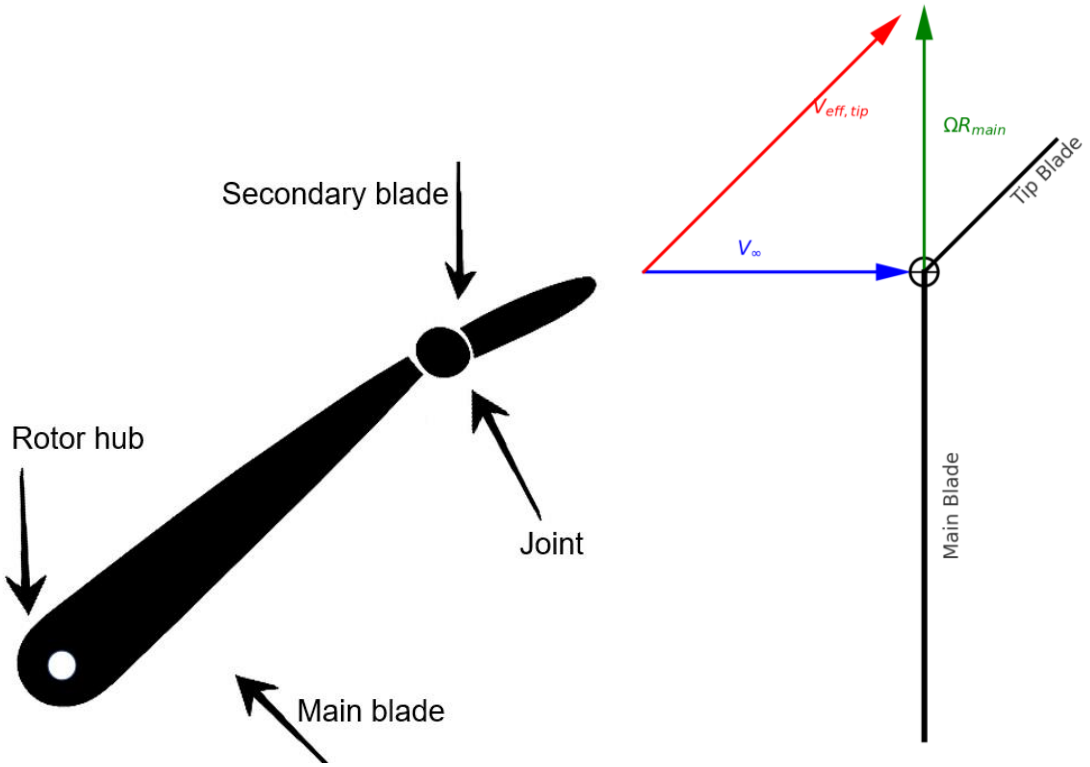

Fig. 1. Schematic diagram of main + tip propeller blade configuration

III. RESULTS

The MATLAB simulation was executed for forward speeds ranging from 0 to 30 m/s in increments that produced 31 discrete performance points. At each point, thrust, power consumption, and propulsive efficiency were computed for both the main and tip-mounted propellers. The Performance Summary Table (Table 1) provides a complete overview of these results.

Table 1. Performance results of the main and tip-mounted propellers

V_∞ (m/s)	T_{main} (N)	T_{tip}(N)	T_{total} (N)	P_{main} (W)	P_{tip} (W)	P_{total}(W)	η_{main}	η_{tip}	η_{total}
0	7.2753	-5.3882	1.887	23.501	37.218	60.719	0	0	0
1	5.9863	-5.3927	0.59357	28.849	37.207	66.056	0.2075	-0.14494	0.0089859
2	4.7489	-5.4062	-0.65722	30.458	37.173	67.631	0.31184	-0.29087	-0.019435
3	3.609	-6.7309	-3.1219	28.828	47.805	76.632	0.37558	-0.4224	-0.12221
4	2.5603	-6.7393	-4.179	24.693	47.382	72.075	0.41475	-0.56893	-0.23192
5	1.617	-6.7731	-5.1561	19.509	47.164	66.674	0.41441	-0.71804	-0.38667
6	0.71475	-6.8191	-6.1043	14.552	46.954	61.506	0.2947	-0.87137	-0.59549
7	-1.4192	-6.3872	-7.8065	1.2111	-0.30692	0.90417	-8.203	145.68	-60.437
8	-2.9279	-7.3261	-10.254	81.642	1.3984	83.04	-0.2869	-41.911	-0.98786
9	-4.8735	-7.9164	-12.79	17.13	4.1675	21.298	-2.5605	-17.096	-5.4048
10	-3.705	-7.1993	-10.904	56.062	-2.7641	53.297	-0.66088	26.045	-2.0459
11	-5.0229	-7.2923	-12.315	-10.453	-3.4142	-13.867	5.2859	23.495	9.7691
12	-4.5897	-7.3931	-11.983	31.252	-4.1574	27.094	-1.7624	21.339	-5.3072
13	-3.0902	-7.5009	-10.591	1.9776	-4.9992	-3.0217	-20.314	19.505	45.566
14	-4.2934	-7.615	-11.908	-60.489	-5.9425	-66.432	0.99368	17.94	2.5096
15	-5.3165	-7.7342	-13.051	-100.1	-6.9723	-107.07	0.79671	16.639	1.8284
16	-5.5163	-7.8332	-13.35	26.936	-7.5031	19.433	-3.2767	16.704	-10.992
17	-6.4833	-8.3566	-14.84	33.278	-0.523	32.755	-3.312	271.63	-7.7019
18	-11.004	-6.7821	-17.786	-157.74	2.9367	-154.8	1.2557	-41.569	2.0682
19	-13.745	-7.0551	-20.8	-158.03	-6.2492	-164.28	1.6526	21.45	2.4057
20	-13.616	-8.2569	-21.873	-219.07	-22.865	-241.93	1.2431	7.2223	1.8082
21	-14.487	-9.6228	-24.109	-341.67	-40.579	-382.25	0.89037	4.9798	1.3245
22	-13.509	-9.1043	-22.613	-277.47	-45.953	-323.42	1.0711	4.3587	1.5382
23	-13.702	-9.0311	-22.733	-171.71	-49.721	-221.43	1.8353	4.1776	2.3613
24	-12.567	-8.6942	-21.262	-142.71	-55.205	-197.91	2.1135	3.7797	2.5783
25	-12.611	-8.41	-21.021	-206.93	-58.751	-265.68	1.5236	3.5787	1.978
26	-17.594	-8.5064	-26.101	-385	-59.6	-444.6	1.1882	3.7108	1.5264
27	-15.803	-8.6083	-24.411	-260.02	-60.495	-320.51	1.641	3.842	2.0564
28	-20.913	-8.0097	-28.923	-572.27	-63.314	-635.58	1.0232	3.5422	1.2742
29	-16.688	-9.5944	-26.282	-115.79	-54.032	-169.82	4.1794	5.1495	4.4881
30	-15.499	-9.629	-25.128	-109.78	-56.247	-166.02	4.2356	5.1358	4.5406

The main propeller exhibits a decreasing thrust trend as forward speed increases, with the decline becoming more pronounced beyond 5 m/s as shown in Fig. 2. In contrast, the tip-mounted propeller produces predominantly negative thrust across the entire range, with the magnitude increasing with speed. This indicates that without pitch optimization, the tip propeller often functions as a parasitic load rather than a thrust-producing element. The crossover region where both thrust curves approach each other marks the onset of significant adverse aerodynamic interaction.

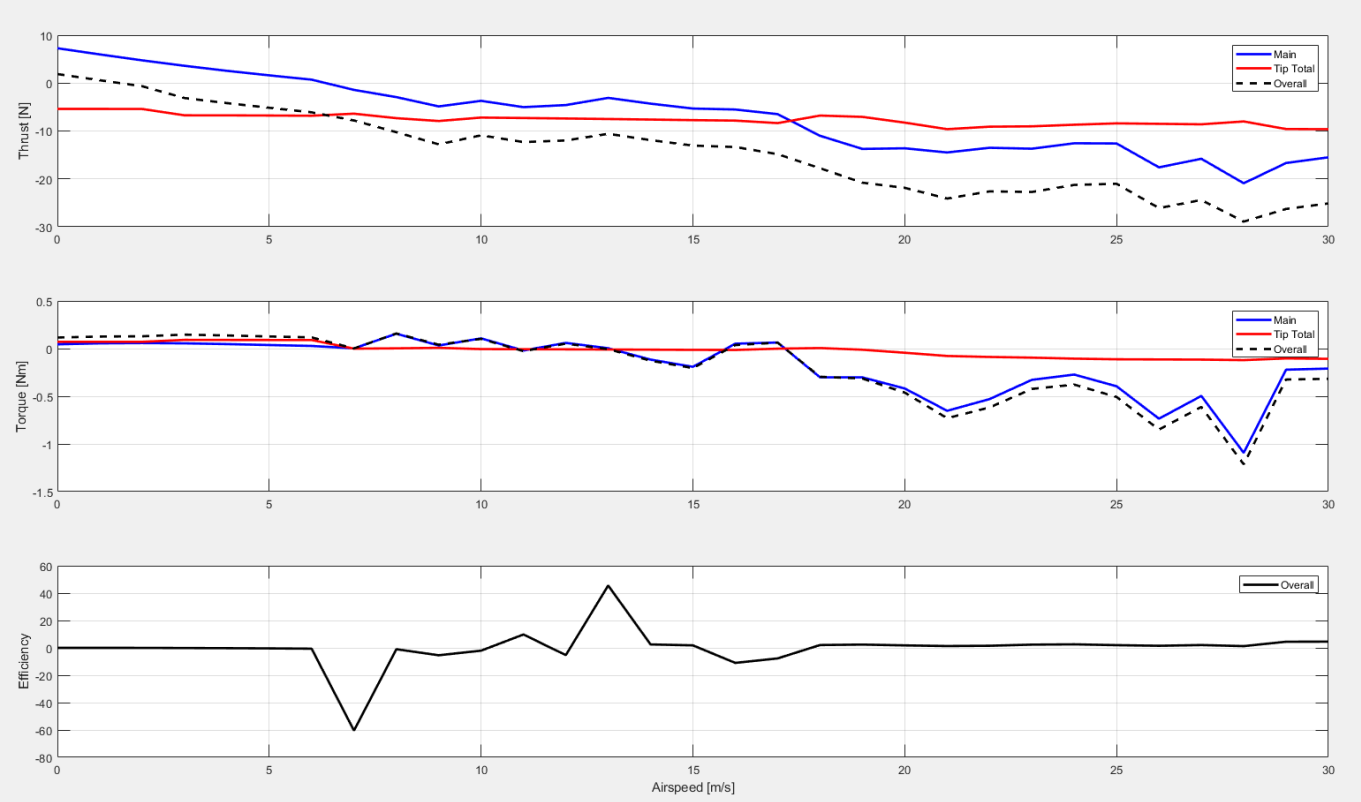

Fig. 2. Thrust, torque and efficiency of the propeller sections.

The combined thrust of the main and tip-mounted propellers demonstrates a net decline as illustrated in Fig. 3, with negative values appearing beyond low advance ratios. The magnitude of total negative thrust in certain speed ranges is substantial, suggesting that the drag penalty from the tip-mounted element outweighs the lift benefit from the main propeller in these regimes. This reinforces the need for adaptive blade pitch or disengagement mechanisms.

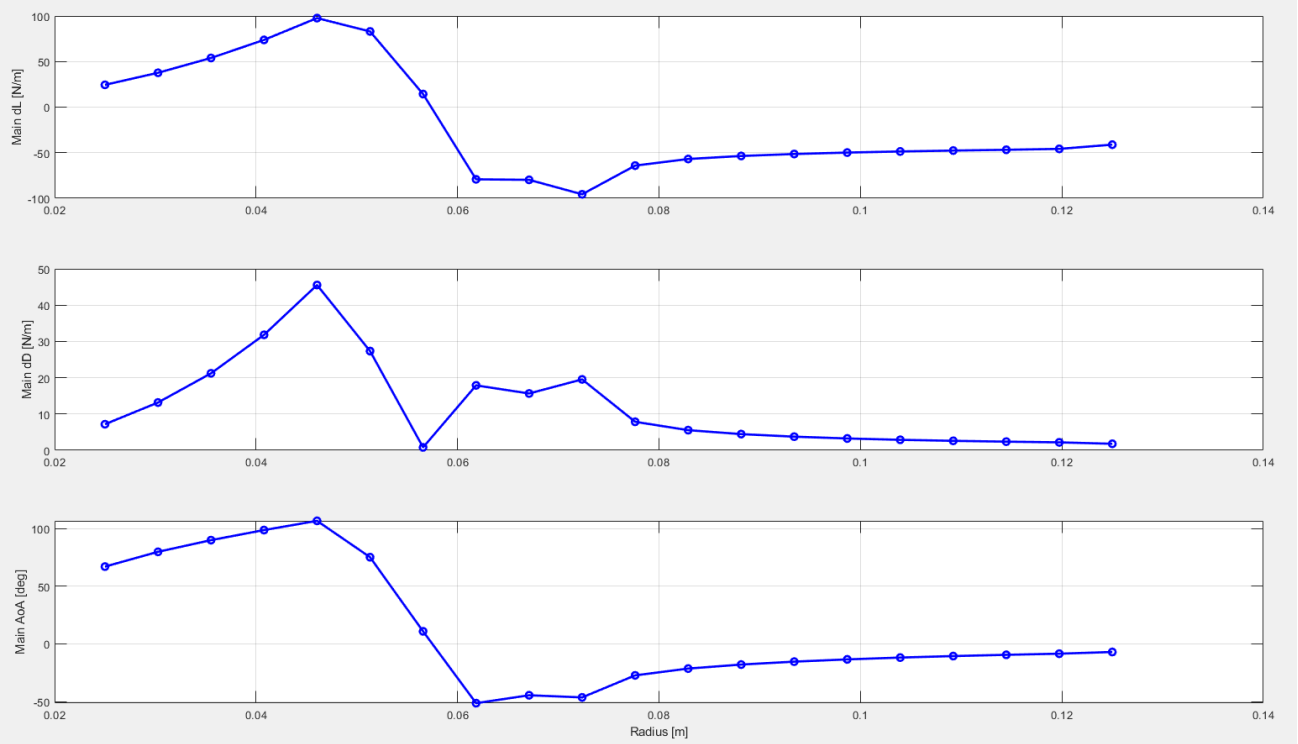

Fig. 4. Elemental performance of main blade on lift, drag.

Main propeller power consumption follows a generally increasing trend until mid-range speeds, after which fluctuations are observed due to the changing inflow angle and induced velocity distribution as shown in Fig. 5. The tip-mounted propeller, however, displays frequent negative power values, indicating energy extraction from the flow. This wind-turbine-like behaviour occurs under conditions where the tip blade's inflow vector aligns unfavourably with its aerodynamic pitch.

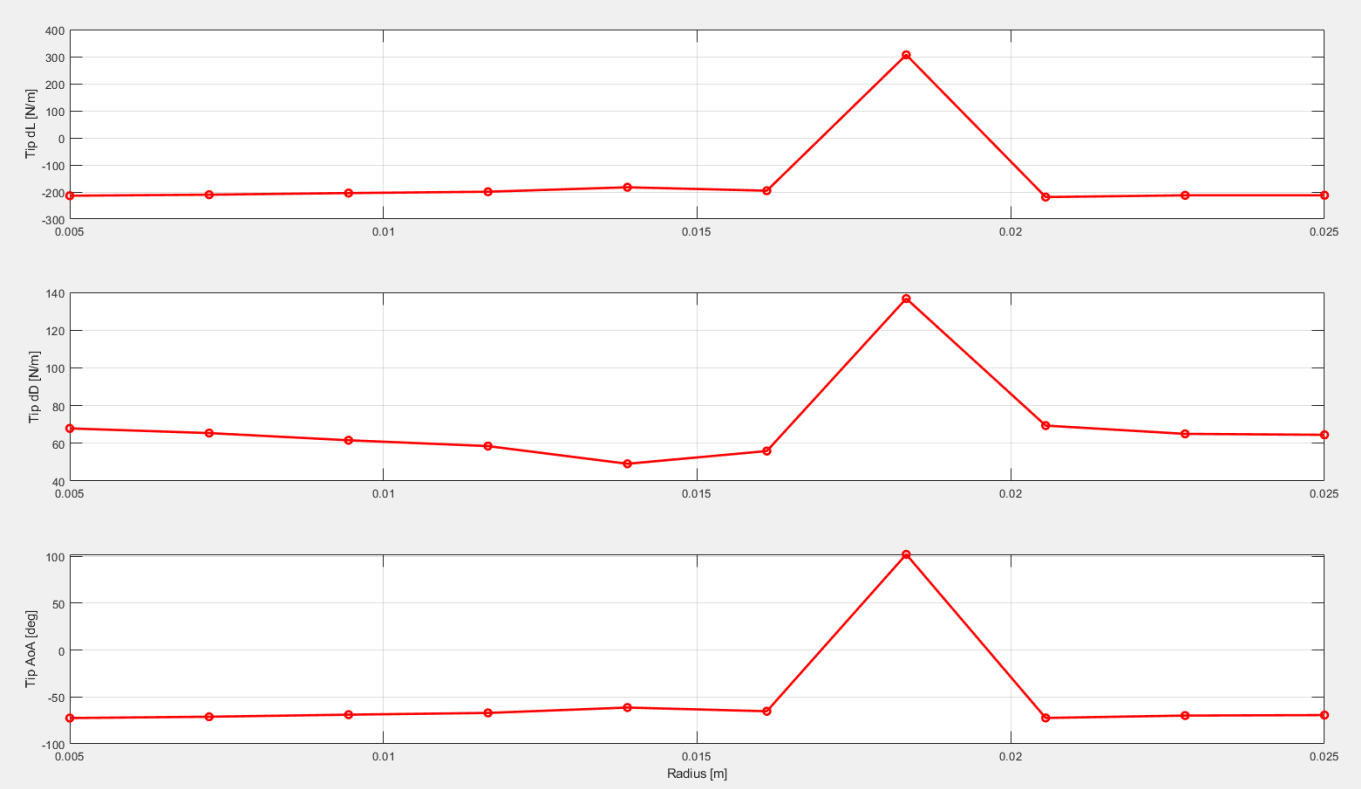

Fig. 5. Elemental performance of tip blade on lift, drag.

IV. DISCUSSION

The numerical results and performance curves presented in Section 3 provide clear evidence of the aerodynamic challenges associated with jointed tip-mounted propellers operating in the tip flow environment of a main blade. The most significant observation is the persistent negative thrust contribution of the tip-mounted blades across most of the tested forward speed range (Table 1, Figures 2–3). This behaviour can be attributed to the combined effects of the high tangential velocity imparted by the main blade rotation and the varying relative inflow direction experienced by the tip blade.

From a momentum theory perspective, the tip-mounted blade operates in a region where the effective freestream velocity $V_{eff,tip}$ is the vector sum of the main blade tangential speed and the aircraft forward velocity:

$$V_{eff,tip} = \sqrt{(V_\infty cos\phi)^2 + (\omega_{main} R_{tip} + V_\infty sin\phi)^2}$$

Where;

ϕ is the inflow angle at the tip and R_{tip} is the main blade tip radius.

This formulation inherently leads to a high advance ratio for the tip propeller, particularly at elevated forward speeds, which explains the frequent transition from thrust production to drag generation.

Another critical finding is the power extraction phenomenon (Figures 4–5), where the tip-mounted propeller sometimes operates in a turbine mode, delivering negative power values. While this might

appear beneficial from an energy recovery standpoint, in reality, the extracted power manifests as increased drag on the main blade, thereby degrading the net thrust. Without an energy conversion system to harness this extracted power (e.g., driving onboard systems or charging storage devices), the effect remains parasitic.

Efficiency analysis (Figures 6–7) underscores the instability of the tip-mounted propeller's performance. Large fluctuations and unrealistic efficiency peaks occur in conditions where the tip thrust magnitude approaches zero, leading to singularities in the η calculation. Such sensitivity suggests that passive fixed-pitch designs are inherently unsuitable for maintaining consistent performance across varied flight regimes.

Comparing these findings to previous studies [3], [6], [8], it is evident that the unfavourable performance of passive tip-mounted blades aligns with experimental observations in mechanically linked or free-spinning designs. However, the present model differs in explicitly computing $V_{eff,tip}$ from vector kinematics rather than assuming purely axial inflow, making the results more physically representative of realistic flight conditions.

From a design perspective, these results indicate that active control of tip-mounted blade pitch — or even the ability to feather or stow the blades during unfavourable operating conditions — could be essential for achieving net benefits. Moreover, there exists potential for hybrid use cases, where the tip-mounted propeller alternates between thrust augmentation during hover/low-speed flight and power generation during high-speed cruise, provided that the energy can be effectively utilized.

Finally, the structural and dynamic implications of adding jointed tip-mounted blades must be considered. The additional mass and aerodynamic loading at the blade tips can influence flutter margins, fatigue life, and vibratory loads on the main rotor hub. These effects, while outside the scope of the present aerodynamic analysis, are critical for practical implementation and warrant future coupled aeroelastic investigations.

V. CONCLUSION

A numerical performance analysis was conducted for a main propeller blade equipped with a jointed tip-mounted propeller, with computations carried out across a broad range of forward speeds. The study employed a kinematic formulation for the effective inflow velocity at the tip-mounted blade, accounting for both the tangential motion of the main rotor and the freestream contribution. This approach enabled realistic prediction of aerodynamic behaviour without relying on simplified purely axial inflow assumptions.

The simulation results reveal several key conclusions:

Negative thrust predominance — Across most of the examined speed range, the tip-mounted propeller produced negative thrust, acting primarily as a drag source. This was especially pronounced at forward speeds exceeding 3–4 m/s, where the effective advance ratio became high due to combined tangential and translational velocity components.

Power extraction phenomena — In several regimes, the tip-mounted propeller exhibited negative power values, effectively operating in a wind-turbine mode. While this represents potential for onboard energy recovery, the associated increase in drag on the main rotor degrades overall propulsive performance unless the recovered energy is effectively utilized.

Efficiency instability — The tip-mounted propeller displayed large fluctuations in calculated efficiency, including unrealistic spikes when thrust approached zero. This instability indicates that passive, fixed-pitch designs are ill-suited for consistent performance across multiple flight regimes.

Overall system degradation — The combined thrust and efficiency of the system were generally inferior to the main propeller operating alone, except in narrow speed intervals where tip contribution was near neutral.

Design implications — For practical adoption, active pitch control, feathering capability, or deployable tip-mounted propellers are recommended. Such control strategies could enable dual-mode operation: thrust augmentation during hover and low-speed flight, and energy harvesting during cruise.

These findings suggest that while the concept of tip-mounted propellers on main rotor blades presents intriguing possibilities, passive configurations are unlikely to yield performance gains without advanced control strategies. Future research should extend the present aerodynamic model by incorporating unsteady aerodynamics, blade–vortex interaction effects, and full aeroelastic coupling to evaluate structural feasibility and vibratory implications.

REFERENCES

[1] S. M. Metev and V. P. Veiko, *Laser Assisted Microtechnology*, 2nd ed., R. M. Osgood, Jr., Ed. Berlin, Germany: Springer-Verlag, 1998.

[2] J. Breckling, Ed., *The Analysis of Directional Time Series: Applications to Wind Speed and Direction*, ser. Lecture Notes in Statistics. Berlin, Germany: Springer, 1989, vol. 61.

[3] S. Zhang, C. Zhu, J. K. O. Sin, and P. K. T. Mok, "A novel ultrathin elevated channel low-temperature poly-Si TFT," *IEEE Electron Device Lett.*, vol. 20, pp. 569–571, Nov. 1999.

[4] M. Wegmuller, J. P. von der Weid, P. Oberson, and N. Gisin, "High resolution fiber distributed measurements with coherent OFDR," in *Proc. ECOC'00*, 2000, paper 11.3.4, p. 109.

[5] R. E. Sorace, V. S. Reinhardt, and S. A. Vaughn, "High-speed digital-to-RF converter," U.S. Patent 5 668 842, Sept. 16, 1997.

[6] (2002) The IEEE website. [Online]. Available: http://www.ieee.org/

[7] M. Shell. (2002) IEEEtran homepage on CTAN. [Online]. Available: http://www.ctan.org/tex-archive/macros/latex/contrib/supported/IEEEtran/

[8] *FLEXChip Signal Processor (MC68175/D)*, Motorola, 1996.

[9] "PDCA12-70 data sheet," Opto Speed SA, Mezzovico, Switzerland.

[10] A. Karnik, "Performance of TCP congestion control with rate feedback: TCP/ABR and rate adaptive TCP/IP," M. Eng. thesis, Indian Institute of Science, Bangalore, India, Jan. 1999.

[11] J. Padhye, V. Firoiu, and D. Towsley, "A stochastic model of TCP Reno congestion avoidance and control," Univ. of Massachusetts, Amherst, MA, CMPSCI Tech. Rep. 99-02, 1999.

[12] *Wireless LAN Medium Access Control (MAC) and Physical Layer (PHY) Specification*, IEEE Std. 802.11, 1997.